ORIGINAL PAPER

Integration of sequence stratigraphy and geostatistics in 3-D reservoir modeling: a case study of Otumara field, onshore Niger Delta

Paul Edigbue · Mary Taiwo Olowokere ·
Peter Adetokunbo · Eniolayimika Jegede

Abstract Sequence stratigraphic concepts for continental settings were assessed to analyze depositional systems of the formations penetrated by wells in the Otumara field. Identification and delineation of five sequences and their bounding surfaces was carried out using well logs. Reservoir sands A to D were mapped using conventional 3-D seismic interpretation techniques. Geostatistical simulation was carried out to provide equiprobable representations of the reservoirs, and the distribution of reservoir parameters and system tracts delineated from the stratigraphic framework. The modeled reservoir properties resulted in an improved description of reservoir distribution and connectivity. Reservoir sands A and B have the highest distribution of both highstand systems tract (HST) and lowstand systems tract (LST) deposits, while reservoir sands C and D have the lowest. Since reservoir sands C and D are from deeper depth, the results indicate that HST and LST decrease with depth while transgressive systems tract (TST) increases with depth. Correlating the 3-D geostatistical model with structures shows prospects with low and high hydrocarbon saturation. Crossplot of porosity and permeability for all reservoirs yielded good correlation. The crossplot of systems tract and hydrocarbon saturation with lithofacies as Z value shows a strong correlation of 0.89. The result also indicates that high hydrocarbon saturation is related to sandy facies of lowstand systems tract. Thus, the LST has the highest hydrocarbon potential. The models resulting from this study can be used to improve reservoir management and well placement, and to predict reservoir performance in Otumara field.

Keywords Sequence stratigraphy · Geostatistics · Simulation · Seismic

Introduction

Modeling of complex reservoirs requires a combination of conceptual stratigraphic models and geostatistical simulations. The approach consists of predicting the overall reservoir geometry and their extension with a stochastic conceptual model. The development of high-resolution stratigraphy has considerably improved our understanding of genetic unit architecture as a function of accommodation variations (Posamentier et al. 1988; Van Wagoner et al. 1987). Application of such methodology at the reservoir scale provides a stratigraphic framework that may reduce the risk of misties between different genetic units. Furthermore, these conceptual models can be used to predict reservoir extent and architecture up to a certain level such as the estimation of channel amalgamation or shoreface sequence extension (Cross et al. 1993). Sand/shale ratios and gross reservoir quality can also be estimated by such an approach. In many cases, conceptual models are essential at the scale of the reservoir unit, but their accuracy commonly remains insufficient to realistically predict the distribution of internal heterogeneities (Haldorsen and Damsleth 1990). Stochastic approaches are now more frequently applied to

P. Edigbue · P. Adetokunbo (✉)
Earth Sciences Department, King Fahd University
of Petroleum and Minerals, Dhahran, Saudi Arabia
e-mail: peterkunbo@gmail.com

P. Edigbue
e-mail: paul_edigbue@yahoo.com

M. T. Olowokere · E. Jegede
Department of Applied Geophysics, Federal University
of Technology, Akure, Nigeria
e-mail: olowo_mt@yahoo.com

simulate the distribution of small-scale sedimentary bodies and internal reservoir heterogeneity (Alabert and Corre 1991; McDonald et al. 1992; Massonnat et al. 1993; Shanor et al. 1993). Geostatistical approaches also provide equiprobable realizations of the heterogeneity distribution. This flexibility can be used to evaluate the impact of different geological scenarios, which contribute to the optimization of a field development plan. The study presented here combines both stratigraphic and geostatistical approaches. Sequence stratigraphic analysis was performed and this resulted in the defining of reservoir layering. Within this framework, geostatistical simulations provide different realizations of the small-scale geological heterogeneities.

Study area and geology

The field is situated a few kilometers north of Warri, Niger Delta. The Niger Delta is situated on the continental margin of the Gulf of Guinea (Fig. 1) and extends throughout the Niger Delta Province (Klett et al. 1997). It occurs at the southern end of Nigeria between latitudes 3° and 6° N and longitudes 3° and 9° E. It covers an area of about 75,000 km². Stable mega tectonic frames such as the Benin and Calabar flanks mark the northwestern and eastern boundaries of the delta, respectively, while the Anambra Basin and the Abakaliki High mark the northern boundary. The delta is bounded in the south by the Gulf of Guinea (Mode et al. 2014).

The Tertiary Niger Delta formed the petroleum system (Kulke 1995; Ekweozor and Daukoru 1984). The sequence consists of alternation of clastic lithologies that occur in combined depositional packages of progradation offlap cycles. These depositional packages comprise of sandstones, silts, and shales of much resemblance, irrespective of their age in the sequence. The stratigraphic sequence consists of massive continental sands of the Benin Formation above 914 m (3000 ft), the paralic sequence of the Agbada Formation (from 914–3658 m) which formed the reservoir units, and Akata Formation below 3658 m (Doust and Omatsola 1990). The Akata Formation is of
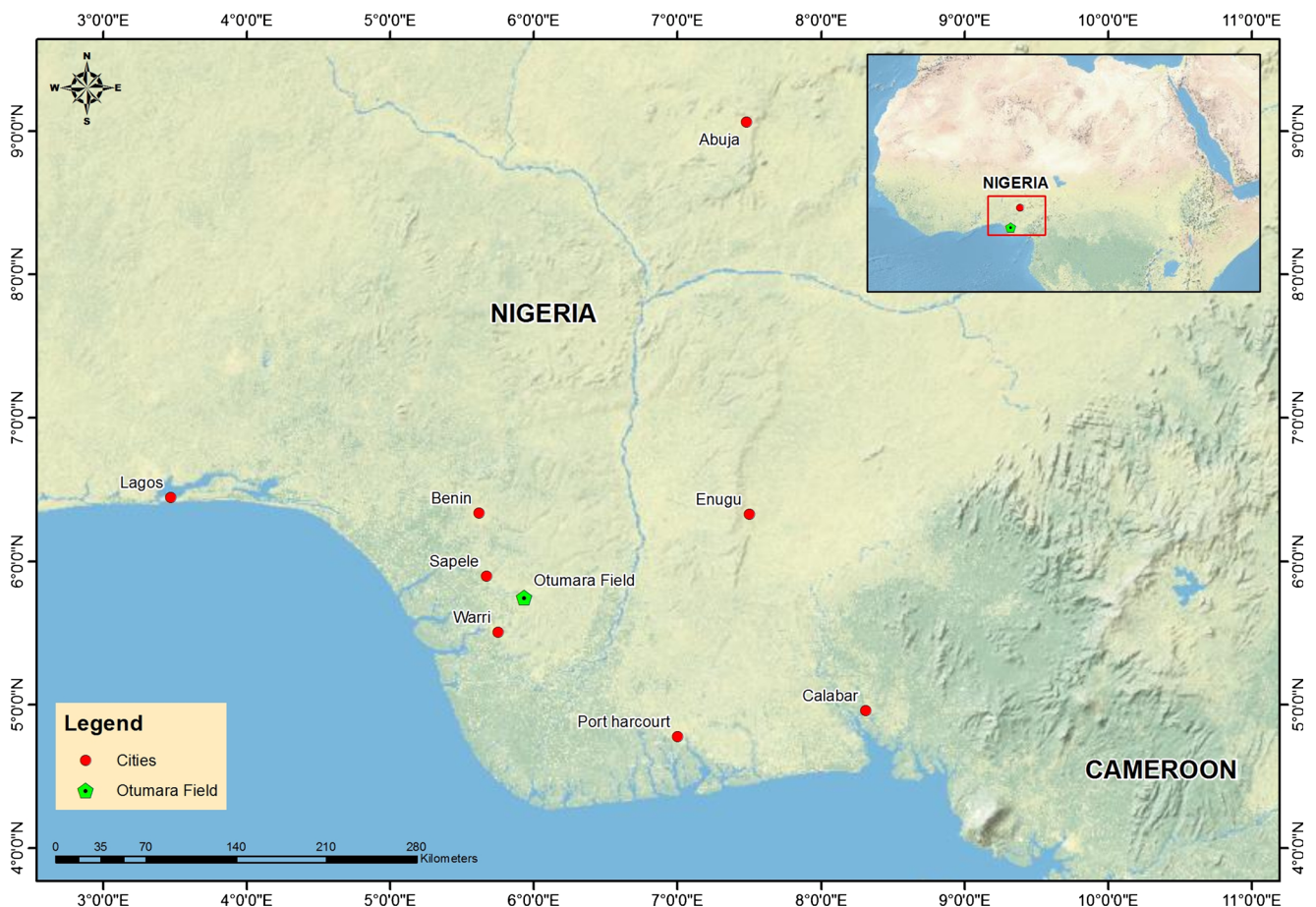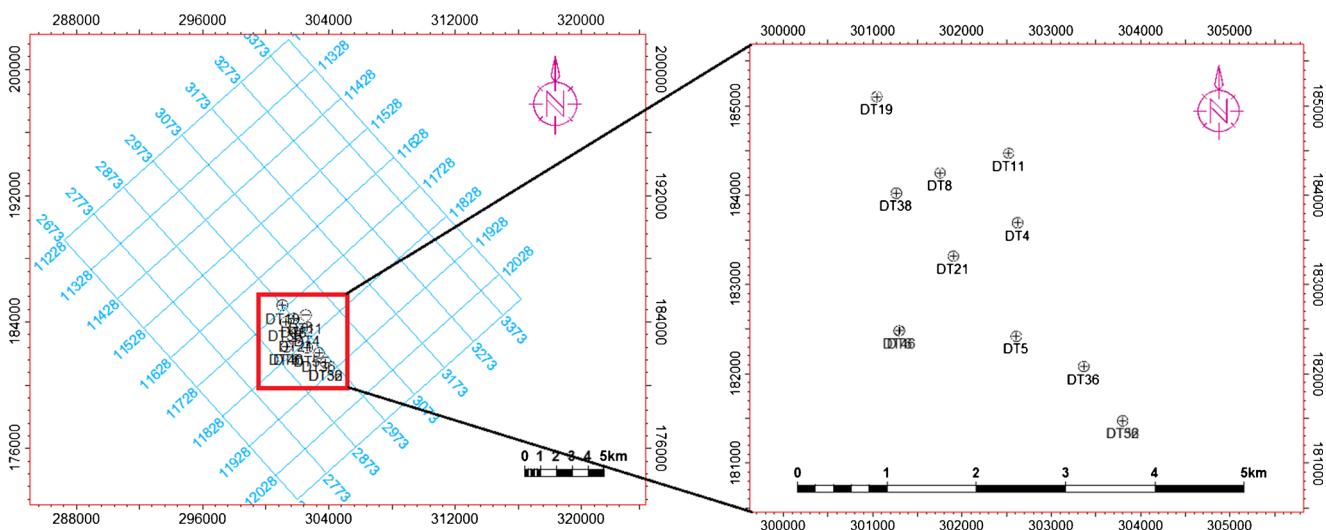

Fig. 1 Location map of the study area

Fig. 2 Stratigraphic column showing the three formations of the Niger Delta (After Shannon and Naylor 1989; Doust and Omatsola 1990)
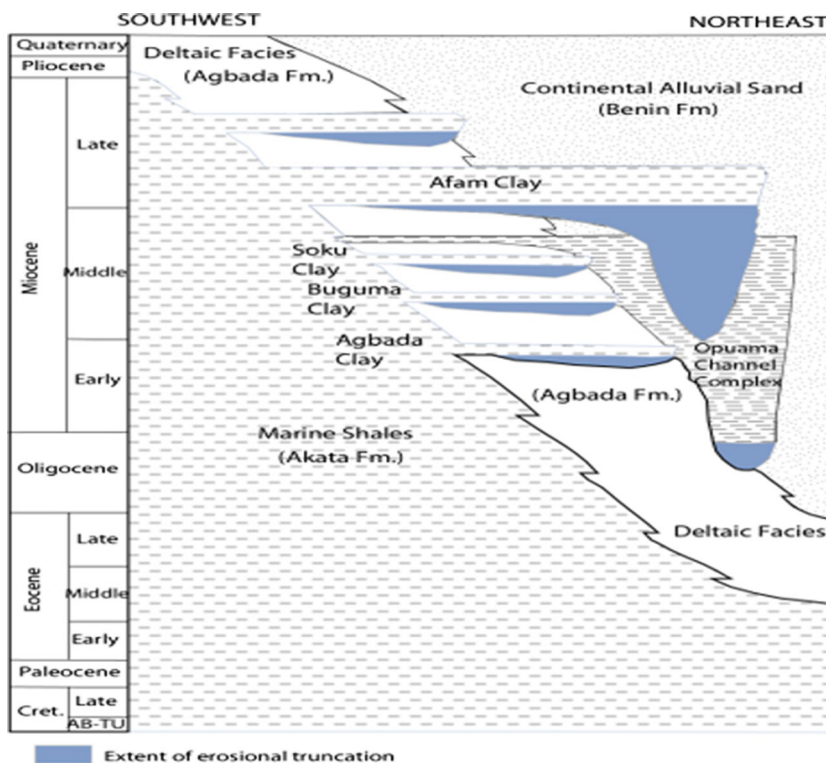
marine origin and composed of thick shale which serves as potential source rocks (Fig. 2). The complete progradation clastic depositional sequence reaches an optimum thickness of 30,000–40,000 ft (9000–12,000 m) at the approximate depocenter in the central part of the delta (Avbovbo 1978; Kulke 1995).

Most of the structural features present in the Niger Delta are caused by the extensional deformation in the sedimentary fill. Basement tectonics played a limited role in the structural evolution of the Niger Delta as its influence was largely limited to the delta farther south, along the Equatorial Atlantic Oceanic fracture zones. Complex interaction between sediment supply rates and subsidence controlled the structures and stratigraphy of the delta. Most visible extensional faulting occurred in the paralic portion of each deltaic sequence (Tuttle et al. 1999; Kogbe 1976). The structure found in the field consists of a simple rollover bounded to the North by a major growth fault and a minor antithetic crestal fault. They are generally of low-relief, elongated anticlinal structures with flank dips of a few degrees. The

Fig. 3 Base map of the study area

Table 1 Lithological classification

Lithology	Code	GR Range (API)
Shale	2	>75
Shaly sand	1	55–65
Sand	0	<55

Table 2 Systems tracts classification

Systems tract	Code	Color
Highstand	0	Green
Transgressive	1	Light brown
Lowstand	2	Yellow

crest is rather flat and the axis that shifts from northeast to southwest, with depth, runs parallel to the bounding fault. The reservoirs chosen for this study were within the Agbada Formation.

Methodology

The data used for this study comprised digital wireline logs (e.g., gamma ray, resistivity, and density logs) from eight wells, check shot, and seismic lines (700 crossline and 600 inline) covering a total area of about 165 km^2. Post-processings such as data cropping and data smoothing with structural preserving algorithms were carried out to improve the quality of the seismic data. Figure 3 shows base map of the study area.

Basic assumptions

In all stratigraphic models, the application of geostatistical methods assume that volumes are conserved between the physical and the chronostratigraphic spaces (Mallet 2004; Prévost et al. 2005); therefore, scale and volume support are not considered. Other primary assumptions are that

the reservoirs are heterogeneous and anisotropic, and the reservoir properties exhibit spatial dependence.

Log estimation: lithologic classification

The Agbada Formation in the Niger Delta is basically made of sand-shale intercalation. Using the defined codes and gamma ray values in Table 1, discrete sand-shale lithologic logs are identified.
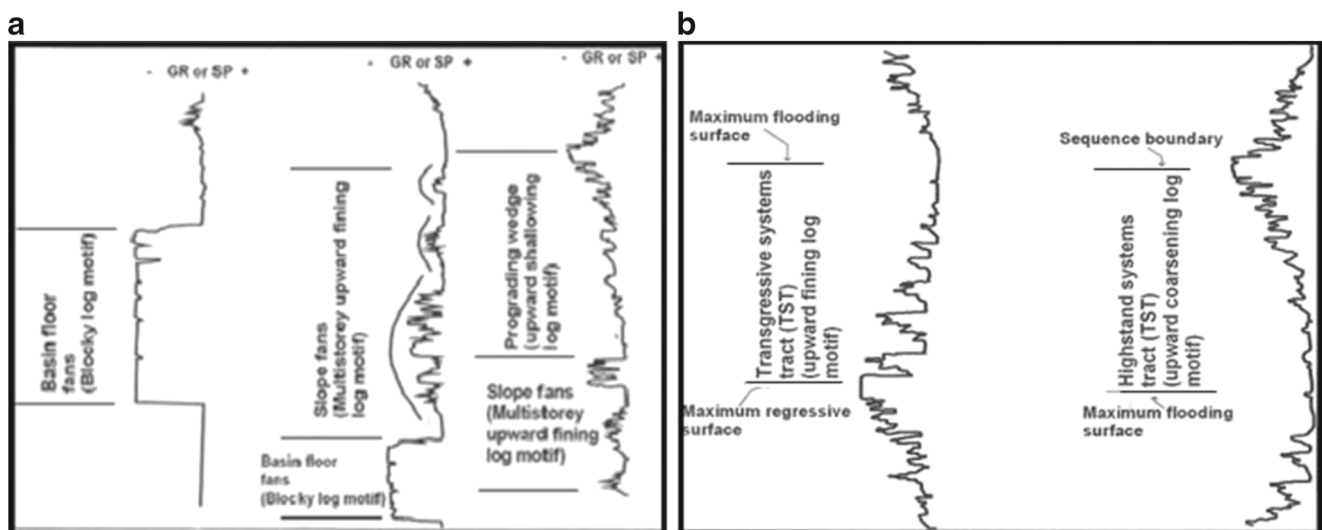
Log estimation: effective porosity

Porosity (ϕ_D) is calculated from the density logs using Eq. 1

$$\phi_D = \frac{\rho_g - \rho_b}{\rho_g - \rho_f} \tag{1}$$

where ρ_g is the grain density (2.65 g/cc), ρ_b is the bulk density from the density log, and ρ_f is the apparent fluid density (1.01 g/cc).The formations are shaly; therefore, effective porosity (ϕ_e) is estimated using Eq. 2 (Dewan 1983).

$$\phi_e = \phi_D - V_{sh}\frac{\rho_g - \rho_{sh}}{\rho_g - \rho_f} \tag{2}$$

a

b

Fig. 4 Log motifs for deposits associated with **a** lowstand systems tracts and **b** transgressive systems tracts and highstand systems tracts (after Vail and Wornardt 1991)
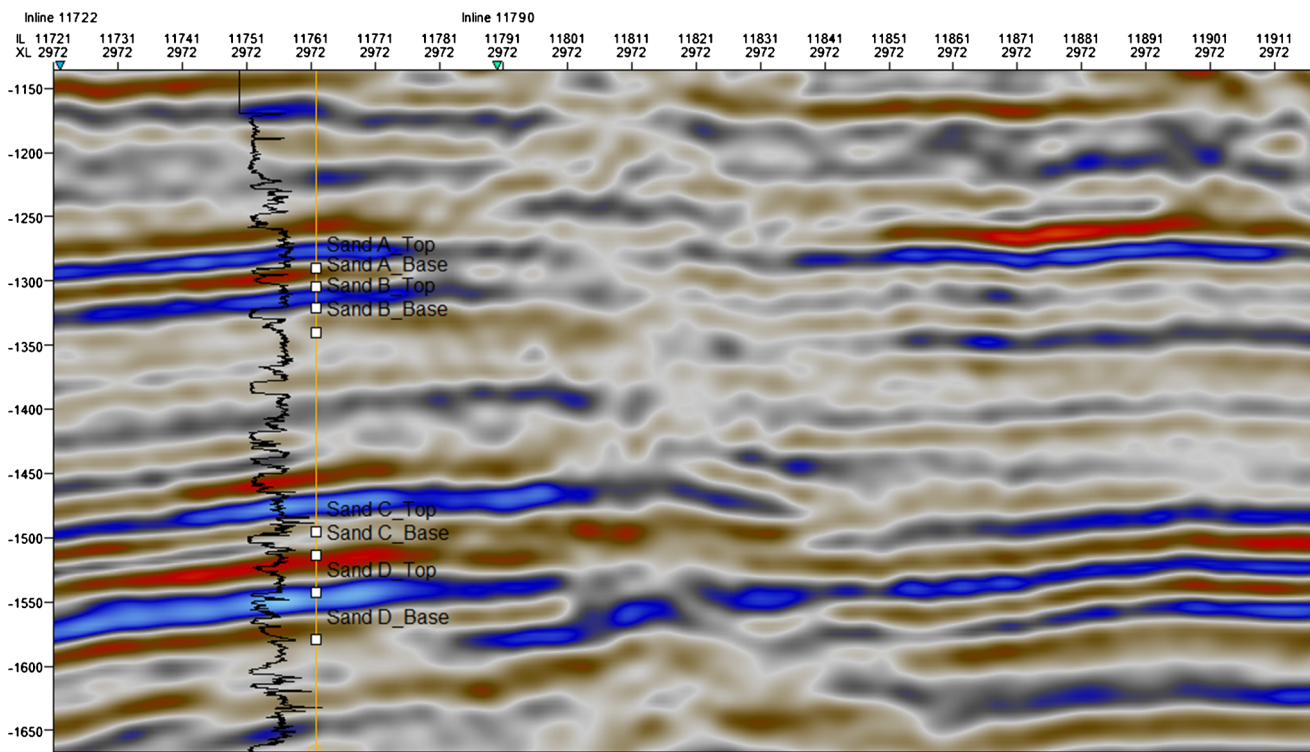
Fig. 5 Well log to seismic tie

where ρ_{sh} and V_{sh} are the density (2.66 g/cc) and volume of shale, respectively. The shale volume V_{sh} is estimated from the gamma ray log.

Log estimation: estimation of true formation resistivity (R_t) and water saturation (S_w)

Deep laterolog (LLD) measures the true resistivity of the formation assuming that the thickness >1 m ($\approx$3 ft) and invasion is not too deep (Asquith and Krygowski 2004). Water saturation is calculated using Eq. 3. The total shale

water saturation model is based on laboratory investigations and field experience which shows that, for many shaly formations, regardless of the shale distribution (laminated or dispersed), this equation works well over the range of S_w normally encountered in the field (Asquith and Krygowski 2004).

$$s_w = \left[\frac{0.4 \times R_w \times (1.0 - V_{sh})}{\phi_e^m} \times \left(\frac{V_{sh}}{R_{sh}} \right)^2 \right.$$

$$\left. + \frac{\phi_e^m}{0.2 \times R_w \times (1.0 - V_{sh}) \times R_t} \right]^{\frac{1}{n}} - \frac{V_{sh}}{R_{sh}} \quad (3)$$
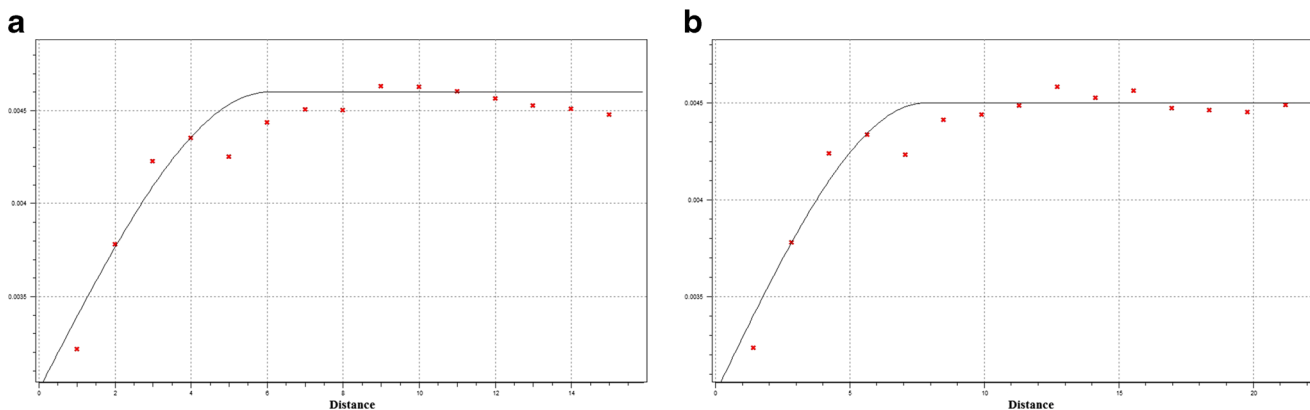
a

b

Fig. 6 Typical variogram. **a** Vertical semivariogram of porosity **b** porosity semivariogram at azimuth 135
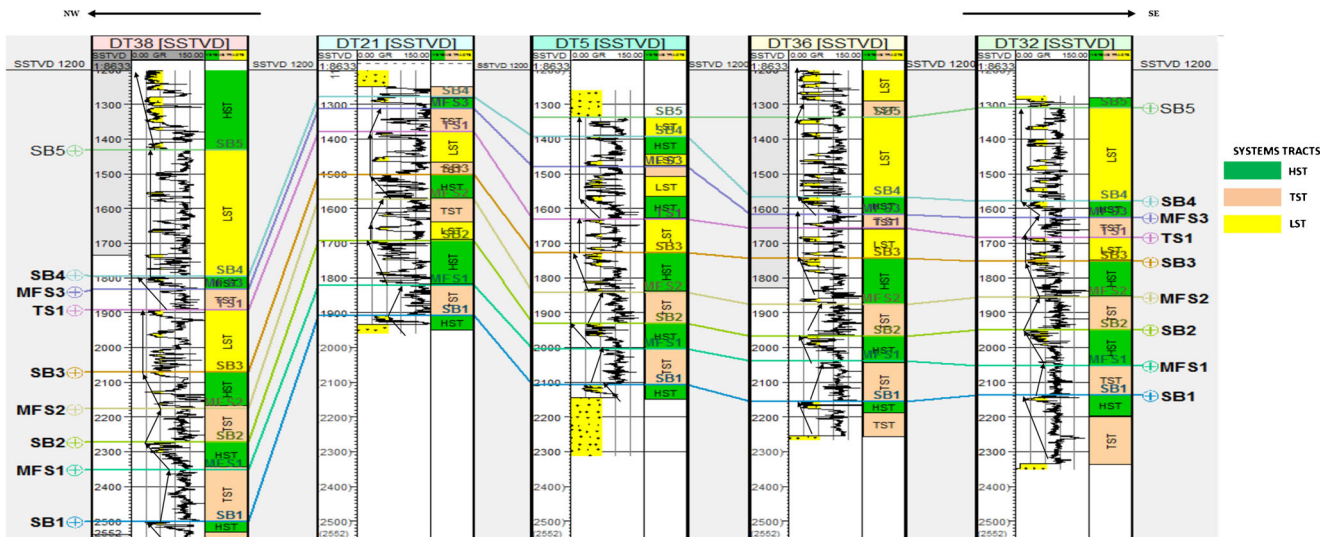
Fig. 7 Well log correlation panel showing along NW-SE direction, stratigraphic frame work and associated log motif
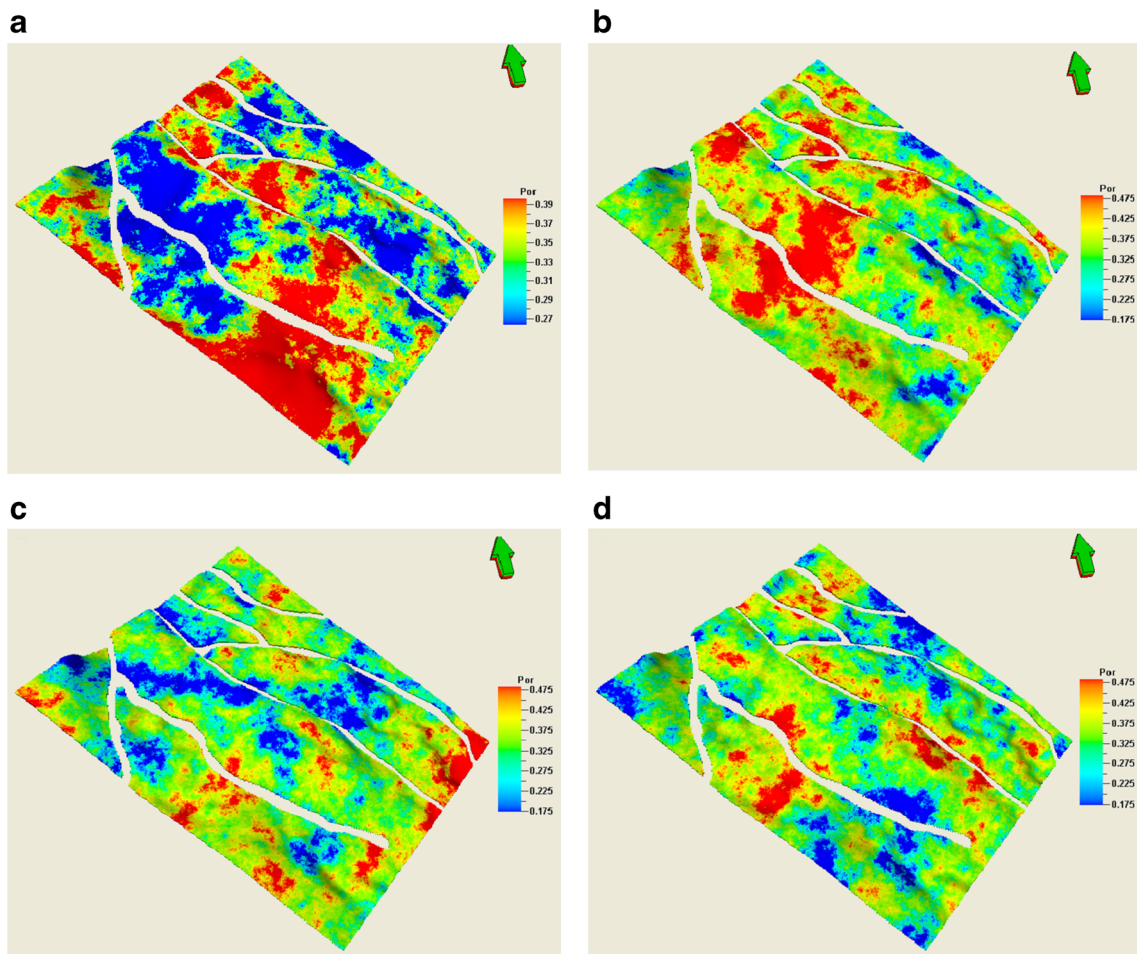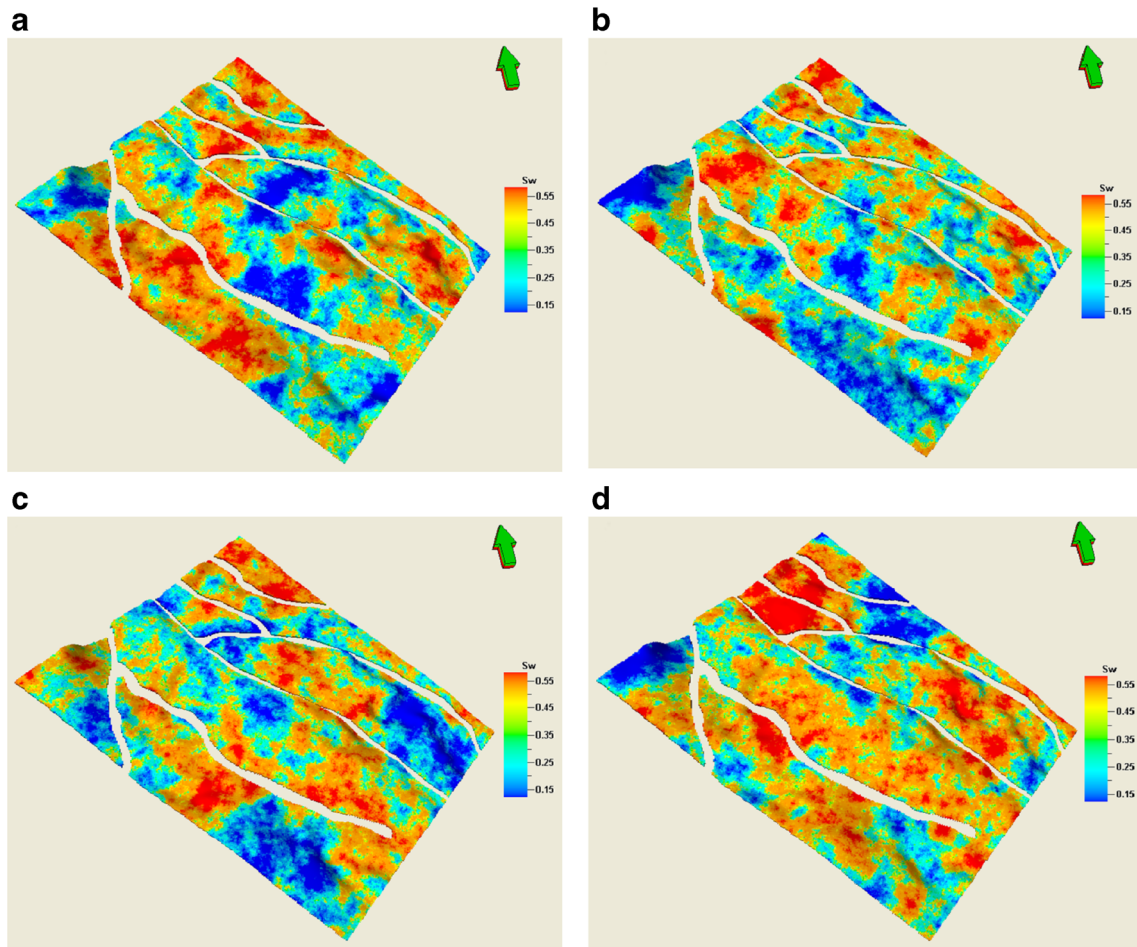

Fig. 8 Typical realizations for porosity generated from sequential Gaussian simulation for reservoir sand A

Fig. 9 Typical realizations for water saturation generated from sequential gaussian simulations for reservoir sand A

where R_w = water resistivity at formation temperature (ohm-m), R_t = resistivity reading on deep log (ohm-m), ϕ_e = effective porosity (fractional), m = cementation exponent (unitless), n = saturation exponent (unitless), R_{sh} = resistivity of the shale (ohm-m), V_{sh} = shale volume (fractional), and S_w = water saturation (fractional)

Log estimation: systems tracts

The stratigraphic units in the Niger Delta are basically made of the Akata, Agbada, and Benin Formations. These units are made up of systems tracts, defined as "three dimensional depositional models that are genetically related and bounded by stratigraphic surfaces" (Van Wagoner, 1995).

Using the gamma ray log motif (Fig. 4) and color codes (defined in Table 2), systems tracts discrete log; lowstand systems tract (LST), transgressive systems tract (TST), and highstand systems tract (HST) logs are identified. Five sequences and their bounding surfaces were analyzed and mapped across wells in the field.

Well log and seismic interpretation

The hydrocarbon reservoirs were mapped based on low gamma ray counts and high resistivity values. Check shot data was used to tie well log with seismic (Fig. 5). The essence of seismic interpretation is to evaluate the quality of the mapped reservoir from the available well log across

Table 3 Statistics summary of realizations for reservoir sand A porosity

Realizations/statistical parameters	1	2	3	4	Real data
Mean	0.3242	0.3644	0.3304	0.3323	0.3421
Standard deviation	0.0879	0.0779	0.0818	0.079	0.0956
Coefficient of variation	0.2711	0.2138	0.2476	0.2380	0.2795

Table 4 Statistics summary of realizations for reservoir sand A water saturation

Realizations/statistical parameters	1	2	3	4	Real data
Mean	0.3946	0.3685	0.3688	0.4234	0.3758
Standard deviation	0.1599	0.1574	0.1660	0.1545	0.1821
Coefficient of variation	0.4052	0.4271	0.4501	0.3649	0.4846

the entire field which later serves as secondary data (top and base limits) for reservoir modeling. Horizons that correspond with reservoir tops from well log were mapped using guided auto tracking techniques. They were converted to time structural maps and subsequently converted to depth contoured map.

Upscaling of well logs

Upscaling is the process where values are assigned to the cells penetrated by the well logs in the 3-D grid. Since each cell can only hold one value, the well logs must be averaged, i.e., the lithology, resistivity, porosity, permeability, water saturation, and systems tracts logs are upscaled into the 3-D grid using the arithmetic mean, the *most-of* and the *neighbour cells* method. The latter two methods utilizes harmonic average with permeability and volume weighted average with both porosity and water saturation. The quality of the upscaled logs is checked by inspecting their histogram produced by the software. This is used for comparing the raw logs with the upscaled logs. If there are no large disparities between them, the upscaled logs are acceptable.

Variogram analysis

A variogram is a quantitative description of a location-dependent property as a function of separation distance (lag) (Fig. 6). The larger the separation distance between two points, the larger the variability. A variogram must be specified when a discrete property is "populated" (that is extrapolated to densely spaced points) using a stochastic simulation algorithm. The variogram analysis was carried out for all zones in three directions. The major direction is northwest–southeast being the trend of the rollover structure in the study area. The minor direction (northeast–southwest, NE-SW) is perpendicular to the major direction while the vertical direction conforms to depth (Fig. 7).
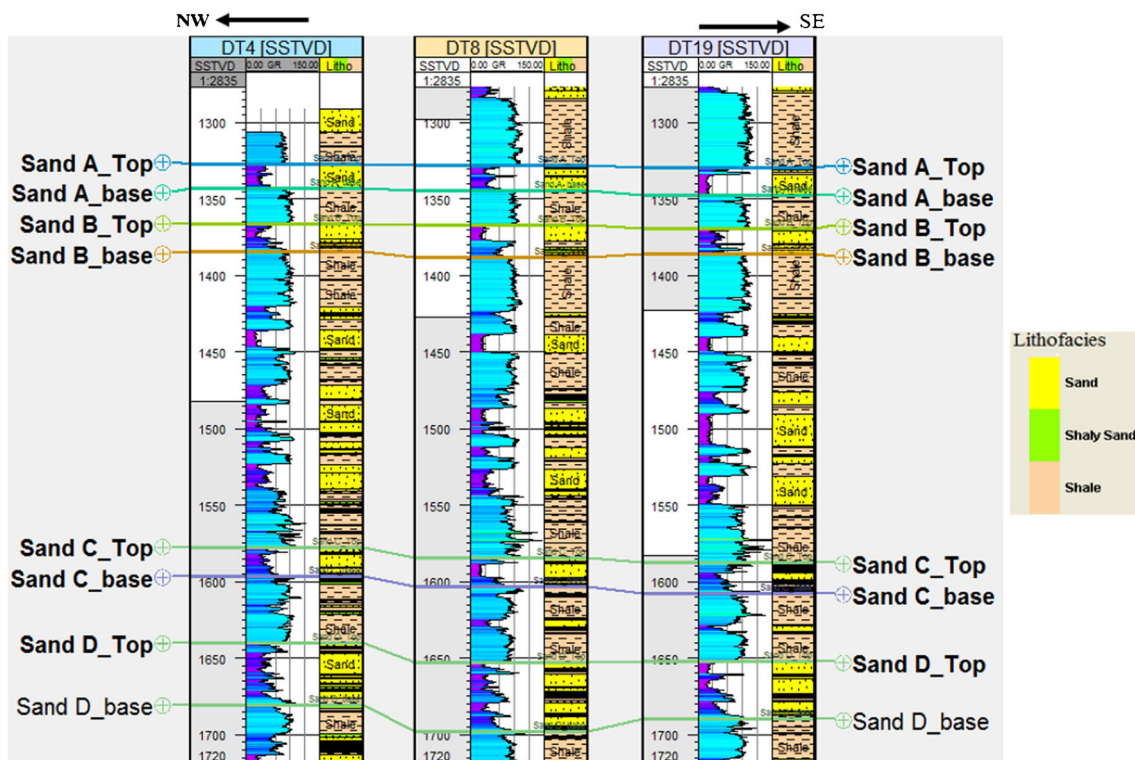
Fig. 10 Sand-shale lithologic logs identified from gamma ray logs

Crossplots and linear regression analysis

Crossplots are the most common bivariate statistical methods that provide the relationship between two variables. Crossplots are used to explore the relationship between sequence elements and relevant reservoir properties such as resistivity, water saturation, permeability, and effective porosity. The crossplots are also used as secondary variable in the co-simulation technique.

Property modeling

The next step involves property modeling. Property modeling is the distribution of reservoir rock properties in 3-D geocellular models using geostatistical principles. 3-D property modeling without adequate data analysis will result in idealistic models/realizations that have little or no relation to geology. Therefore, a good understanding of the nature of the input data is central to meaningful property modeling. The proper tool for this is the variogram analysis for each zone.

Stochastic simulation

Stochastic simulation is a method of generating multiple equally probable realizations of reservoir properties (Esfahani and Asghari 2013), rather than simply estimating the mean (as in kriging). Sequential Gaussian simulation (SGS), one of the dominant forms of stochastic simulation for reservoir modeling applications, was utilized. The algorithm was used to generate several and equiprobable realizations (Figs. 8 and 9) that honor the local conditioning (well) data, the global histogram, areal and vertical geological trends of the data and patterns of spatial correlation. The best realization was picked based on statistical similarity with the actual data (Tables 3 and 4).

Results

The resultant univariate, bivariate, and 3-D models of the reservoir properties are presented in this section. The univariate models involve the variograms while the bivariate
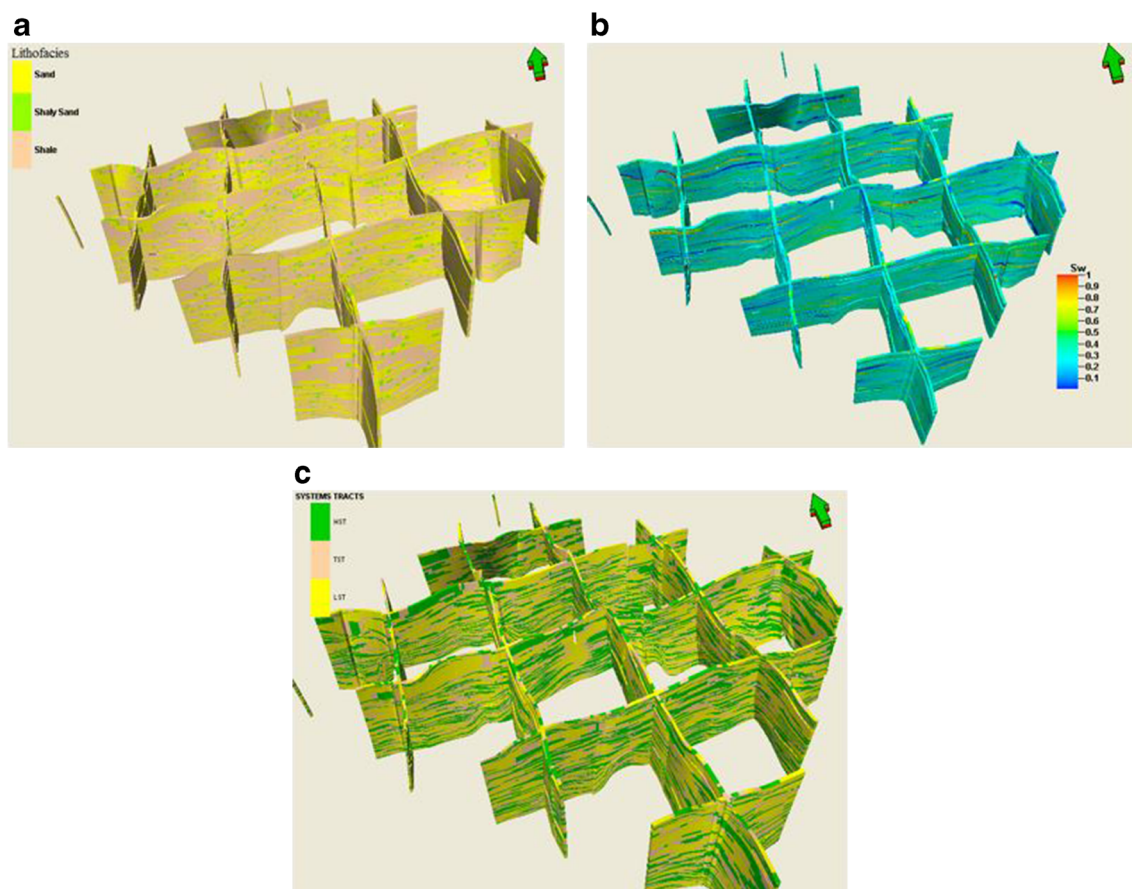

Fig. 11 Models under investigation. **a** Fence diagram of lithology showing shale continuity in the study area. **b** Fence diagram of water saturation showing low water saturation anomaly continuity in the study area. **c** Fence diagram of systems tracts showing lateral continuity in the study area

models involve the crossplots. The 3-D models show the result of the three-dimensional sequential Gaussian simulation.

Lithology model of the reservoir

The estimated lithologic log (Fig. 10) shows that the vertical and lateral continuity of the interbedded and intra-reservoir

shale laminae are considerable. The fence diagram of the lithology (Figs. 11 and 12 shows a complete interpreted seismic section with all the mapped faults.) accentuates the vertical and areal continuity of the interbedded and intra-reservoir shale laminae. Relatively thin (6–30 m) reservoirs are separated by thick (12–50 m) and expansive shale units. Sands C and D reservoirs appear to have more shale content than sands A and B reservoirs. The intra-reservoir shale
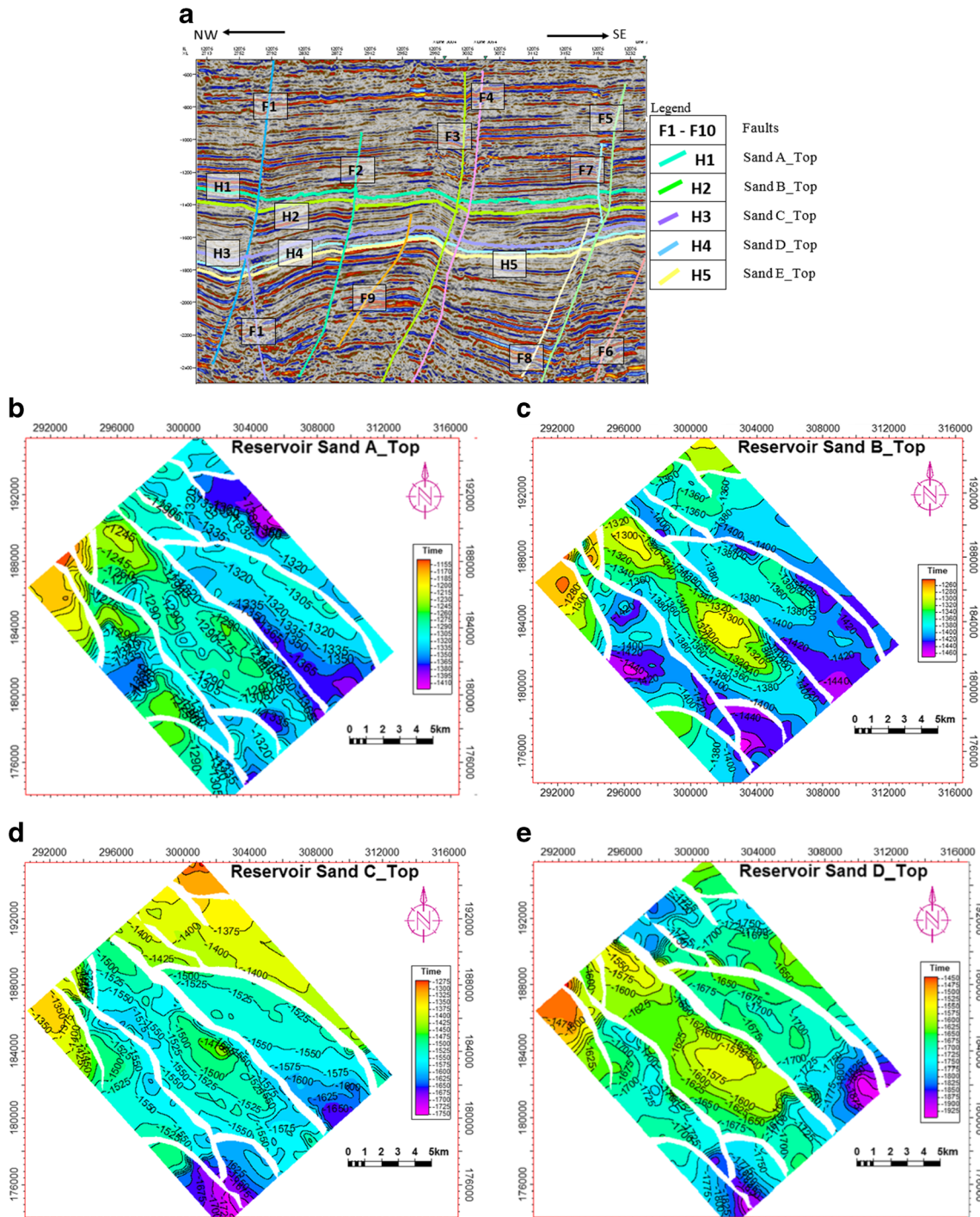
Fig. 12 **a** Interpreted section and time structure maps of **b** reservoir sand A, **c** reservoir sand B ,**d** Reservoir sand c, and **e** reservoir sand D

Table 5 Mean reservoir properties

Reservoirs	Mean thickness (m)	Mean water saturation	Mean volume of shale	Mean porosity
Sand A	22.00	0.17	0.21	0.48
Sand B	21.00	0.20	0.53	0.45
Sand C	29.50	0.25	0.48	0.42
Sand D	43.50	0.21	0.74	0.37

laminae depict distinct lateral terminations in the models. Table 5 shows the summary of the reservoir properties computed across all reservoirs of interest. It has been deduced that volume of shale decreases from reservoir sand A to D which is the deepest reservoir. This shows that shallow reservoirs contain less shale than the deepest ones. All reservoirs show good reservoir properties which indicate that they are productive.

Water saturation models

Figure 11b is the fence diagram showing both the lateral and vertical variation of water saturation in all the reservoirs. Water saturation varies from 0.14–0.65 in reservoir sand A, 0.20–0.60 in reservoir sand B, 0.17–1.0 in reservoir sand C, and 0.20–0.83 in reservoir sand D. The 3-D geocellular models of water saturation in the reservoirs are
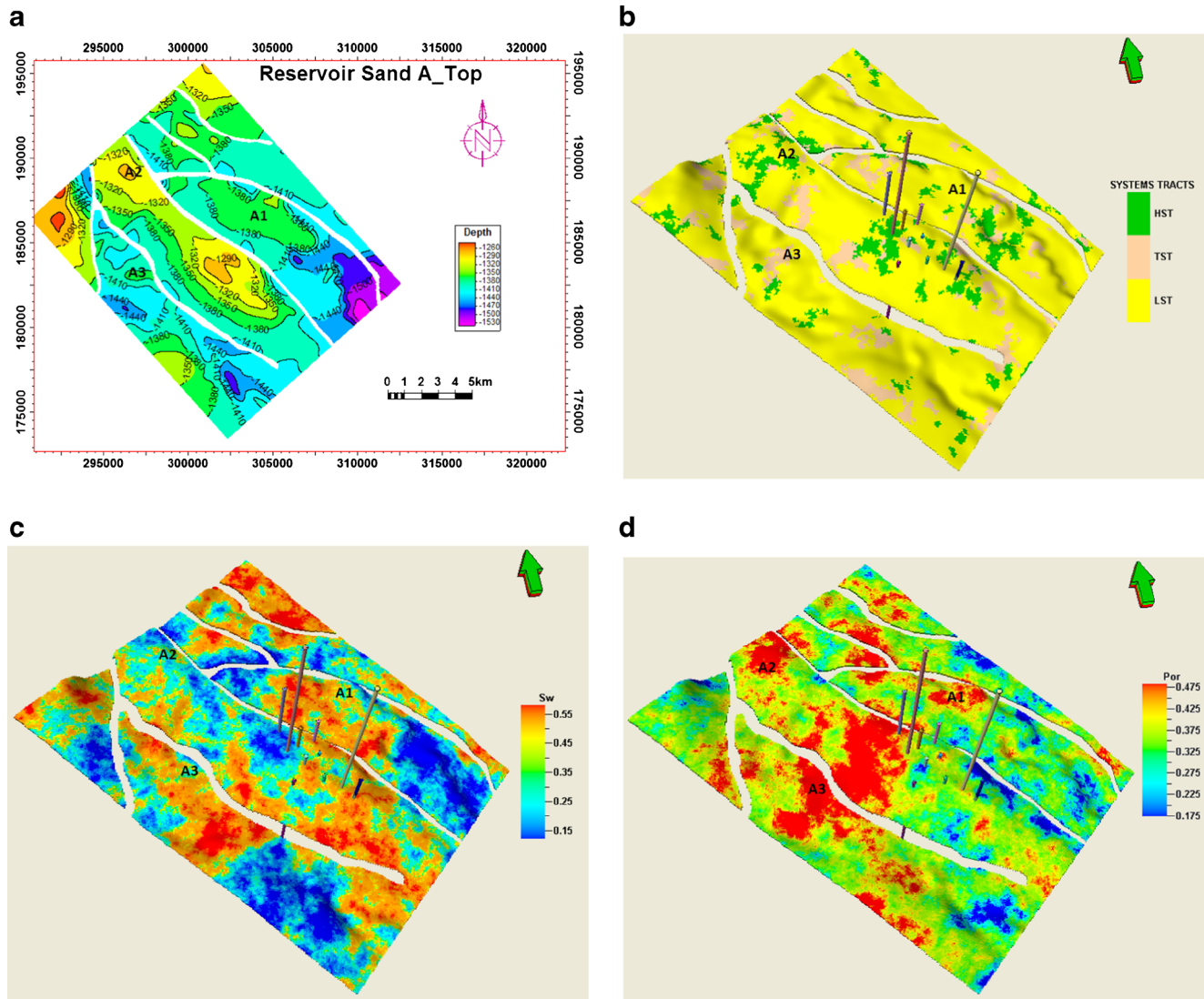
Fig. 13 Correlation of 3-D geocellular model with structures on reservoir sands A, A1, A2, and A3 are delineated prospects. **a** Structural map. **b** System tracts model. **c** Water saturation model. **d** Porosity model

shown in Figs. 13c, 14c, 15c, and 16c. The average water saturation is 0.42, 0.51, 0.62, and 0.55 for reservoirs sands A, B, C, and and D, respectively. The standard deviation is 0.19, 0.18, 0.21, 0.19, and 0.23 for sands A, B, C, D, and E, respectively. These results show that these reservoirs are hydrocarbon bearing and that reservoir sand A appears to have the highest hydrocarbon saturation. It is followed by reservoir sand B.

A close examination of the maps show the area of structural high (anticline) depicted by closures and their associated faults (growth fault and antithetic fault) that can possibly trap hydrocarbon. The maps also show tested closures (with wells) and the untested closures, which are the prospects. Prospects A1, A2, and A3 were delineated on reservoir sand A, prospects B and C were delineated on

Sands B and C reservoir maps respectively, while prospects D1 and D2 were delineated from sand D reservoir map. Structural traps delineated are either anticlinal or fault traps. Most of them are fault-assisted or fault-dependent closures.

Structural maps

Figures 13a, 14a, 15a and 16a show the depth structural map of all interpreted horizons.

Systems tracts models of the reservoirs

The 3-D geocellular models of systems tracts are shown in Figs. 13b, 14b, 15b, and 16b. Statistical analysis shows that HST distribution is about 40 %, TST is about 10 %,
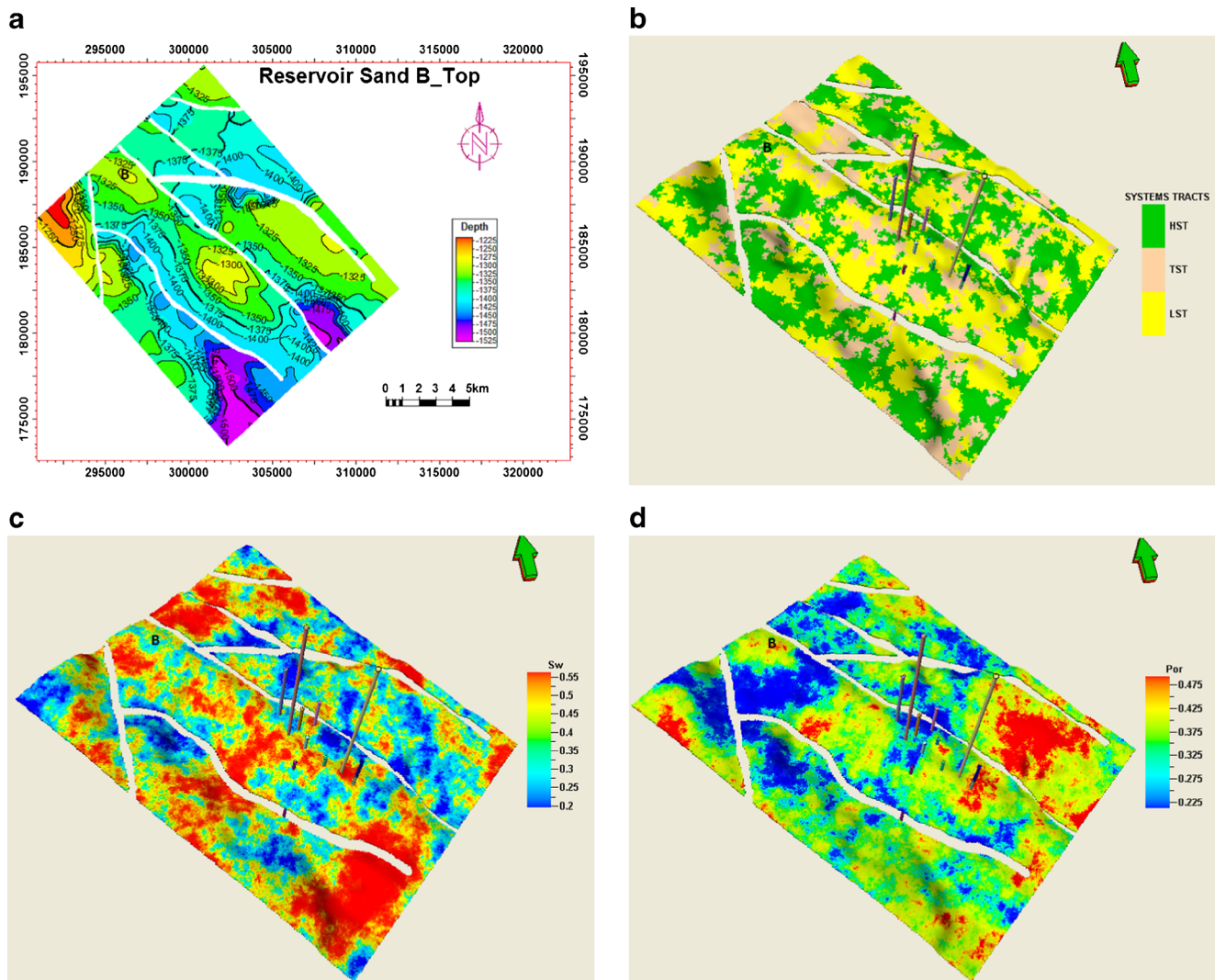
Fig. 14 Correlation of 3-D geocellular model with structures on reservoir Sand B. **a** Structural map. **b** Systems tracts model. **c** Water saturation model. **d** Porosity model
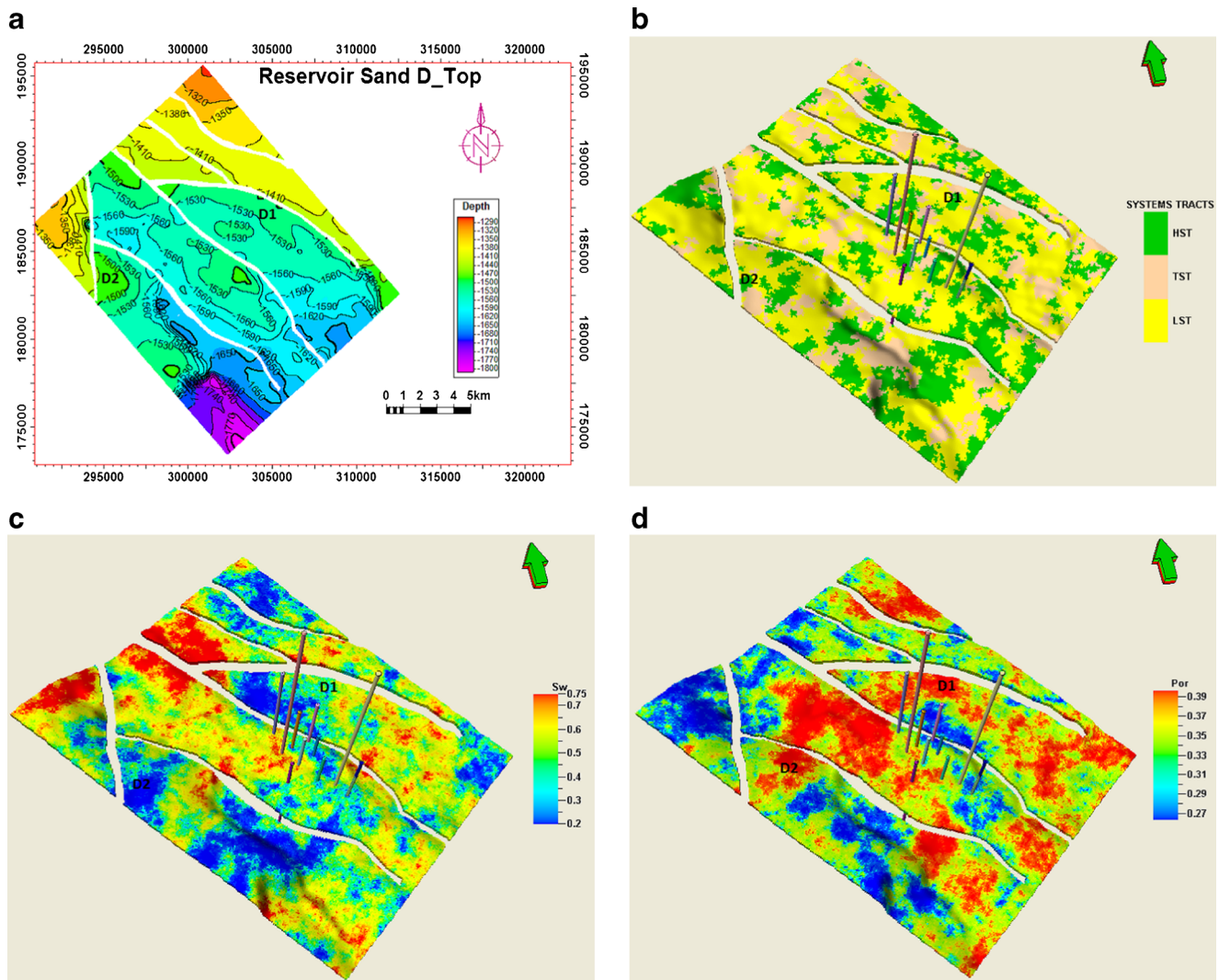
a

b

c

d
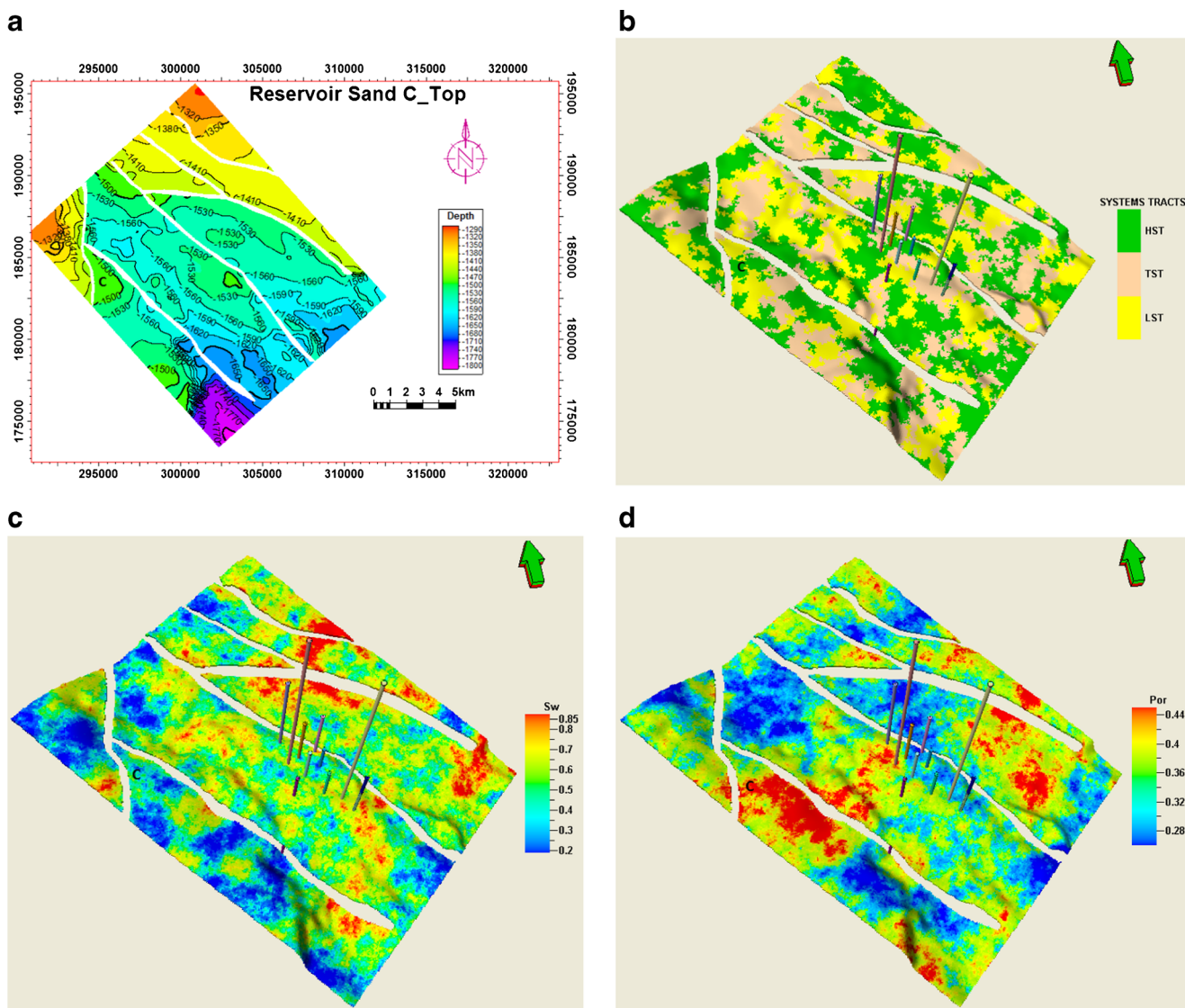
Fig. 15 Correlation of 3-D geocellular model with structures on reservoir Sand C. **a** Structural map. **b** System tracts model. **c** Water saturation mode. **d** Porosity model

and LST is about 50 % in reservoir sand A. Reservoir sand B has the following system tracts distribution; 35 % HST, 15 % TST and 50 % LST. Reservoir Sand C has HST distribution of about 27 %, TST of about 23 %, and LST of about 50 %. Reservoir sand D has HST distribution of about 30 %, TST of about 25 %, and LST of about 45 %. Reservoir sands A and B have the highest distribution of both HST and LST deposits, while reservoir sands C and D has the lowest. Since reservoir sands C and D are from deeper depth, the results indicate that the HST and LST decreases with depth while the TST increases with depth. The result of the fence diagram conforms to the statistical analysis.

Models of effective porosity distribution

The 3-D geocellular models of effective porosity in the reservoirs are shown in Figs. 13d, 14d, 15d and 16d. Statistical analysis of the distributions shows that effective porosity varies from 0.1–0.49, 0.2–0.54, 0.10–0.54, and 0.16–0.45 in reservoir sands A, B, C, and D, respectively. The average effective porosity is 0.48, 0.45, 0.42, and 0.37 for sands A, B, C, and D reservoirs, respectively. The standard deviation is approximately 0.16, 0.14, 0.08, and 0.04 for the reservoirs. Hence, sands A and B reservoir appear to have higher effective porosity than reservoir sand D. The low effective porosity of sand D reservoir is attributed to its high

Fig. 16 Correlation of 3-D geocellular model with structures on reservoir Sand D. **a** Structural map. **b** System tracts model. **c** Water saturation model. **d** Porosity model

shale content. These results show that effective porosity varies spatially within the reservoirs. The degree of variability is higher with depth. These models reveal the influence of lithology and shaliness on the distribution of effective porosity in the reservoirs.

Crossplots of petrophysical properties and facies

Crossplots are generated for porosity and permeability which yields good correlation. Petrophysical parameters are then super imposed on them as the Z values. The results are shown in Fig. 17. Reservoir quality is primarily determined by porosity and permeability, crossplot of these properties for all reservoirs yielded fair correlation (correlation coefficient = 0.47). The result shows that the high-quality reservoir could be separated from low-quality reservoir.

Analysis of the crossplot results shows that the crossplot of porosity and permeability with resistivity as Z value, show area of high resistivity anomaly which corresponds to the high quality reservoir. The crossplot of porosity and permeability with water saturation as Z value shows area of low water saturation anomaly which corresponds to the high-quality reservoir. The crossplot of porosity and permeability with lithofacies as Z value shows area of sand/shaly-sand anomaly which corresponds to the high-quality reservoir. The crossplot of porosity and permeability with system tracts as Z value shows area of high-quality system tracts anomaly which corresponds to the high-quality reservoir. This result also indicate that all the sequence elements could be hydrocarbon bearing. The crossplot of system tract and hydrocarbon saturation with lithofacies as Z-value shows a strong correlation of 0.89. The result also indicates that
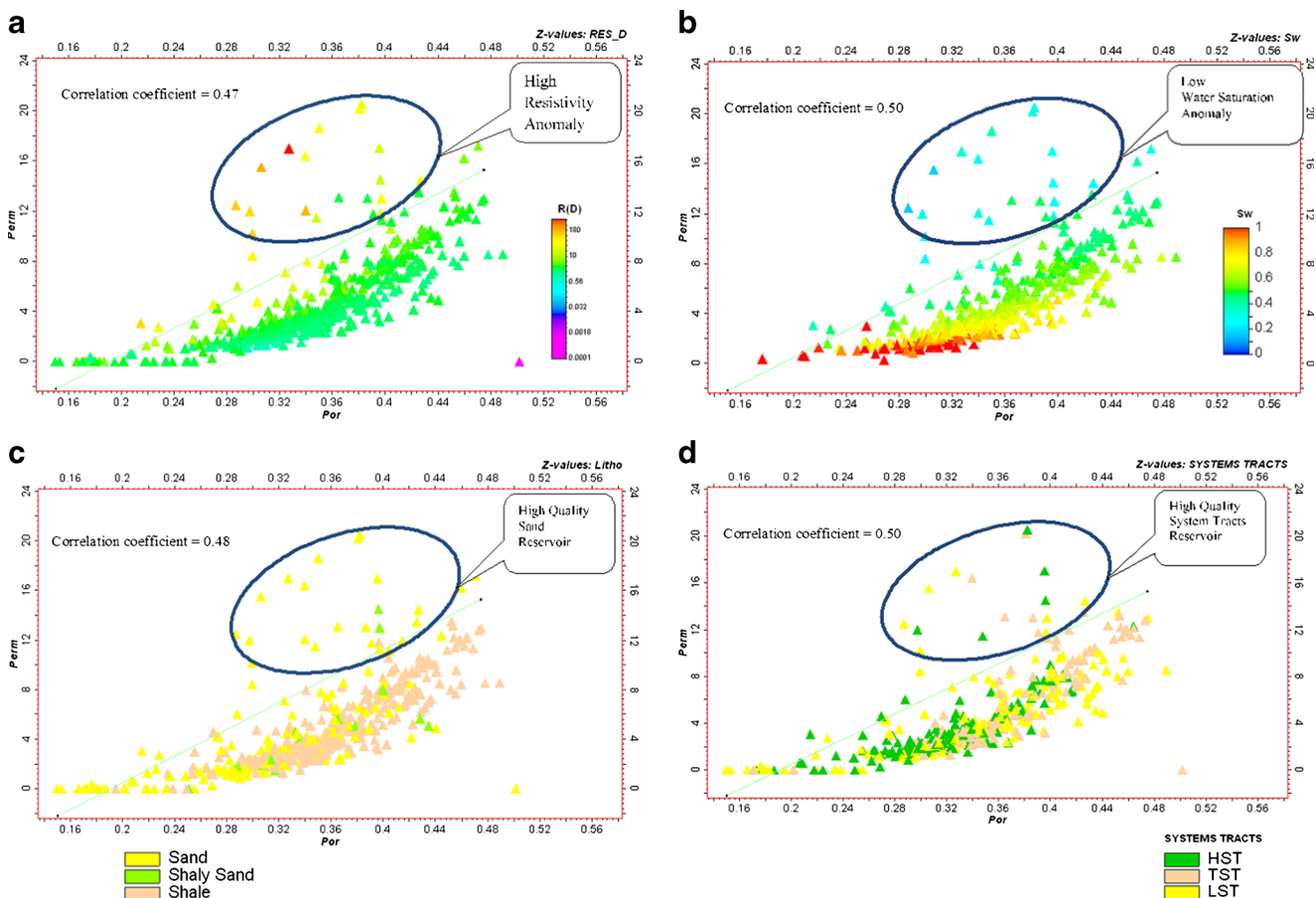
Fig. 17 Crossplot of petrophysical parameters. **a** Crossplot of permeability and porosity with resistivity as *Z* values. **b** Crossplot of permeability and porosity with water saturation as *Z* values. **c** Crossplot of permeability and porosity with lithology as *Z* values. **d** Crossplot of permeability and porosity with systems tracts as *Z* values

high hydrocarbon saturation is related to the sandy facies of lowstand systems tract. Thus, the LST has the highest hydrocarbon potential.

Discussion

The 3-D geocellular models for porosity, water saturation and system tracts were put together with their corresponding structural map for each reservoir sands for the purpose of correlation. Figures 13-16 show the results of the correlation for all the delineated prospects. The result of correlation for reservoir Sand A shows that the porosity model strongly conforms with structure (delineated prospects A1, A2 and A3), while the water saturation model shows that prospect A3 highly conforms with water saturation model, prospect A1 moderately conforms with water saturation model and prospect A2 poorly conforms with water saturation model. However, all the prospects conform to the portion where the HST and LST are about 80 % on the system tracts

geocellular model. The result of correlation for reservoir Sand B shows that the porosity model strongly conforms to delineated prospect B, while the water saturation model shows that prospect B moderately conforms to water saturation model. Also prospect B conforms to the portion where the HST and LST are about 80 % of the system tracts model.

The result of correlation for reservoir Sand C shows that the porosity model strongly conforms to delineated prospect C, while the water saturation model shows that prospect C moderately conforms to the water saturation model. Also prospect C conforms to portion where the LST is about 70 % of the system tracts model. The result of correlation for reservoir sand D shows that the porosity model strongly conforms to delineated prospect D2, while it poorly conforms to delineated prospect D1. The water saturation model shows that prospect D2 highly conforms to the water saturation model, while prospect D1 poorly conform to it. However, prospect D2 conforms to the portion where the HST and LST are about 90 %

while prospect D1 conform to the portion where the HST and LST are about 60 % of the systems tracts geocellular model. This analysis shows that prospects A3 and D2 have high hydrocarbon saturation, prospects A1, B and C have moderate hydrocarbon saturation, while prospects A2 and D1 have poor hydrocarbon saturation. The result also shows that all the delineated prospects have moderate reservoir quality except prospect D1 which has poor reservoir quality.

Conclusion

This work has provided a 3-D spatial distribution pattern of sequence elements and has established the presence of positive system tracts anomalies in the study area. The petrophysical correlation panel generation from this study delineates hydrocarbon bearing reservoir which formed zone of interest for geostatistical and sequence analysis. The property logs that delineated the reservoir zone were computed from the related logs using empirical formula. Stratigraphic frameworks used for equiprobable generation of the delineated reservoirs were created using depositional models from gamma ray log motif. This resulted in a successful sequence analysis and delineation of sequence elements such as HST, TST, and LST in the study area. Geostatistical analysis, variogram models, and stochastic simulation provide equiprobable representation of the geologic heterogeneity within the delineated reservoir units. This made the lateral prediction of both reservoir properties and sequence elements feasible. The generated cross-plots do not only establish the correlation among reservoir properties, but also provided the criteria for mapping a high-quality hydrocarbon reservoir in the study area. The research was completed by building an integrated reservoir model that was based on sequence stratigraphy and geostatistical approaches. These results have significant implications on petroleum exploration and reservoir characterization.For hydrocarbon exploration, the results stress the relevance of sequence elements mapping as a powerful exploration tool. Lowstand deposits with high porosity and permeability are associated with hydrocarbon accumulations. For oilfield development and reservoir characterization, this research has established the relationship between system tracts, effective porosity, lithology and hydrocarbon saturation in the study area. However, drilling of more wells is recommended to validate and/or update the models. The static reservoir models may serve as input for flow simulation. Ultimately, the stratigraphic models will facilitate the estimation of reliable electro–sequence logs honoring effective porosity, saturation and lithology for any part of the oilfield.

References

Alabert FG, Corre B (1991) Heterogeneity in a complex turbiditic reservoir: impact on field development. Society of Petroleum Engineers Annual Technical Conference and Exhibition, SPE paper 22902

Asquith G, Krygowski D (2004) Basic well log analysis, 2nd edition. AAPG Methods in Exploration Series 28

Avbovbo AA (1978) Tertiary lithostratigraphy of Niger Delta. AAPG Bull 62:295–300

Cross TA, Baker MR, Chapin MA, Clark MS, Gardner MH, Hanson, MS, Witter DN (1993) Applications of high-resolution sequence stratigraphy to reservoir analysis. COLLECTION COLLOQUES ET SEMINAIRES-INSTITUT FRANCAIS DU PETROLE 51:11–11

Dewan JT (1983) Essentials of modern openhole log interpretation. Pennwell Publishing, Oklahoma

Doust H, Omatsola E (1990) Divergent and passive basin of the Niger Delta. AAPG Mem 48:239–248

Ekweozor CM, Daukoru EM (1984) Petroleum source bed evaluation of Tertiary Niger Delta–reply. Am Assoc Pet Geol Bull 68:390–394

Esfahani NM, Asghari O (2013) Fault detection in 3D by sequential Gaussian simulation of Rock Quality Designation (RQD) Case study: Gazestan phosphate ore deposit, Central Iran. Arab J Geosci 6(10):3737–3747. doi:10.1007/s12517-012-0633-3

Haldorsen HH, Damsleth E (1990) Stochastic modeling. JPT 42(4):404–412. doi:10.2118/20321-PA. SPE-20321-PA

Klett TR, Ahlbrandt TS, Schmoker JW, Dolton JL (1997) Ranking of the world's oil and gas provinces by known petroleum volume: US Geological Survey Open-file Report, pp 97–463

Kogbe CA (1976) Geology of Nigeria. Elizabethan Publishing Company

Kulke H (1995) Regional petroleum geology of the world. Part II: Africa, America, Australia and Antarctica. Berlin, GebrÃijder Borntraeger, pp 143–172

MacDonald AC, HÃÿye TH, Lowry P, Jacobsen T, Aasen JO, Grindheim AO (1992) Stochastic flow unit modelling of a North Sea coastal-deltaic reservoir. First Break 10(4):124–133

Mallet JL (2004) Space-time mathematical framework for sedimentary geology. Math Geol 36(1):1–32

Massonnat G, Alabert F, Guidicelli C (1993) Anguille Marine, a deep sea-fan reservoir offshore Gabon: from geology to stochastic modelling. SEG Technical Program Expanded Abstracts 1993:345–345. doi:10.1190/1.1822480

Mode AW, Anyiam OA, Aghara IK (2014) Identification and petrophysical evaluation of thinly bedded low-resistivity pay reservoir in the Niger Delta. Arab J Geosci. doi:10.1007/s12517-014-1348-4

Posamentier HW, Jervey MT, Vail PR (1988) Eustatic control on clastic deposition I conceptual framework, sea-level changes: an integrated approach. SEPM Spec Publ 42:109–124

Prévost M, Lepage F, Durlofsky L, Mallet JL (2005) Unstructured 3d gridding and upscaling for coarse modelling of geometrically complex reservoirs. Pet Geosci 11(4):339–345

Shannon PM, Naylor D (1989) Petroleum basin studies. Graham and Trotman Limited, London, pp 153–169

Shanor GG, Bahman S, Bagherpour H, Karakas M, Buck S, Carnegie A, Crossouard PA, Nasta V (1993) An integrated reservoir characterization study of a giant Middle East oil field: part 1–geological modelling. Proceedings of 8th Middle East Oil Show and Conference. SPE Paper 2(25657):491–504

Tuttle ML, Charpentier RR, Brownfield ME (1999) The Niger Delta petroleum system: Niger Delta province, Nigeria, Cameroon, and Equatorial Guinea, Africa. US Department of the Interior, US Geological Survey

Vail PR, Wornardt WW (1991) An integrated approach to exploration and development in the 90s: well log-seismic sequence stratigraphy analysis. Gulf Coast Association of Geological Societies Transactions 41:430–650

Van Wagoner JC, Mitchum RM, Posamentier HW, Vail PR (1987) Seismic stratigraphy interpretation using sequence stratigraphy. AAPG Stud Geol 1(27):11–14